Geophys. J. Int. (2003) **155,** 126–138

GPS constraints on Africa (Nubia) and Arabia plate motions

S. McClusky,[1] R. Reilinger,[1] S. Mahmoud,[2] D. Ben Sari[3] and A. Tealeb[2]

[1]*Department of Earth, Atmospheric, and Planetary Sciences, MIT, Cambridge,* MA 02139, *USA. E-mail: simon@chandler.mit.edu*
[2]*NRIAG, Helwan, Cairo, Egypt*
[3]*Ecole Mohammadia d'Ingenieurs, Rabat, Morocco*

Accepted 2003 April 25. Received 2003 April 8; in original form 2002 September 16

SUMMARY

We use continuously recording GPS (CGPS) and survey-mode GPS (SGPS) observations to determine Euler vectors for relative motion of the African (Nubian), Arabian and Eurasian plates. We present a well-constrained Eurasia–Nubia Euler vector derived from 23 IGS sites in Europe and four CGPS and three SGPS sites on the Nubian Plate ($-0.95 \pm 4.8^\circ$N, $-21.8 \pm 4.3^\circ$E, $0.06 \pm 0.005^\circ$ Myr^{-1}). We see no significant (>1 mm yr^{-1}) internal deformation of the Nubian Plate. The GPS Nubian–Eurasian Euler vector differs significantly from NUVEL-1A ($21.0 \pm 4.2^\circ$N, $-20.6 \pm 0.6^\circ$E, $0.12 \pm 0.015^\circ$ Myr^{-1}), implying more westward motion of Africa relative to Eurasia and slower convergence in the eastern Mediterranean. The Arabia–Eurasia and Arabia–Nubia GPS Euler vectors are less well determined, based on only one CGPS and three SGPS sites on the Arabian Plate. The preliminary Arabia–Eurasia and Arabia–Nubia Euler vectors are $27.4 \pm 1.0^\circ$N, $18.4 \pm 2.5^\circ$E, $0.40 \pm 0.04^\circ$ Myr^{-1}, and $30.5 \pm 1.0^\circ$N, $25.7 \pm 2.3^\circ$E, $0.37 \pm 0.04^\circ$ Myr^{-1}, respectively. The GPS Arabia–Nubia Euler vector differs significantly from NUVEL-1A ($24.1 \pm 1.7^\circ$N, $24.0 \pm 3.5^\circ$E, $0.40 \pm 0.05^\circ$ Myr^{-1}), but is statistically consistent at the 95 per cent confidence level with the revised Euler vector reported by Chu & Gordon based on a re-evaluation of magnetic anomalies in the Red Sea ($31.5 \pm 1.2^\circ$N, $23.0 \pm 2.7^\circ$E, $0.40 \pm 0.05^\circ$ Myr^{-1}). The motion implied in the Gulf of Aqaba and on the Dead Sea fault (DSF) by the new GPS Nubia–Arabia Euler vector (i.e. ignoring possible Sinai block motion and possible internal plate deformation) grades from pure left lateral strike-slip in the Gulf and on the southern DSF with increasing compression on the central and northern DSF with relative motion increasing from 5.6 to 7.5 mm yr^{-1} (± 1 mm yr^{-1}) from south to north. Along the northern DSF (i.e. north of the Lebanon restraining bend) motion is partitioned between 6 ± 1 mm yr^{-1} left-lateral motion parallel to the fault trace and 4 ± 1 mm yr^{-1} fault-normal compression. Relative motions on other plate boundaries (including the Anatolian and Aegean microplates) derived from the GPS Euler vectors agree qualitatively with the sense of motion indicated by focal mechanisms for large crustal earthquakes ($M > 6$). Where data are available on fault-slip rates on plate bounding faults (North Anatolian fault, East Anatolian fault, Dead Sea fault, Red Sea rift), they are generally lower than, but not significantly different from, the full plate motion estimates suggesting that the majority of relative plate motion is accommodated on these structures.

Key words: geodynamics, lithospheric deformation, plate tectonics, satellite geodesy.

INTRODUCTION AND TECTONIC SETTING

Fig. 1 shows the present-day plate configuration in the zone of interaction of the African, Arabian and Eurasian plates. The early (pre-Miocene) history of the Mediterranean and Middle East region is very complex, involving a number of phases of collision, basin formation and accretion of island arcs and continental fragments (e.g. Dercourt *et al.* 1986; Dewey *et al.* 1989). The region underwent a major change during the Late Oligocene (∼35 Ma) when the prior dominance of northward subduction of the Neo-Tethys was replaced by the first stages of continental collision and the development of the Alpine fold and thrust belt, although earlier collision occurred in the Eocene (∼60 Ma) along the Alps in association with the Apulia promontory (Italy/Adriatic). Plate reconstructions indicate that rifting of the Red Sea and separation of the African and Arabian plates was well established by the Early Miocene (∼25 Ma) (e.g. Dercourt *et al.* 1986; Joffe & Garfunkel 1987; Steckler *et al.* 1988). The present-day plate configuration was initiated during the Middle Miocene (∼15 Ma) with initiation of left-lateral motion along the Gulf of Aqaba and Dead Sea fault (DSF) (e.g. Quennell 1984; Hempton 1987; Lyberis 1988; Steckler *et al.* 1998), the principal

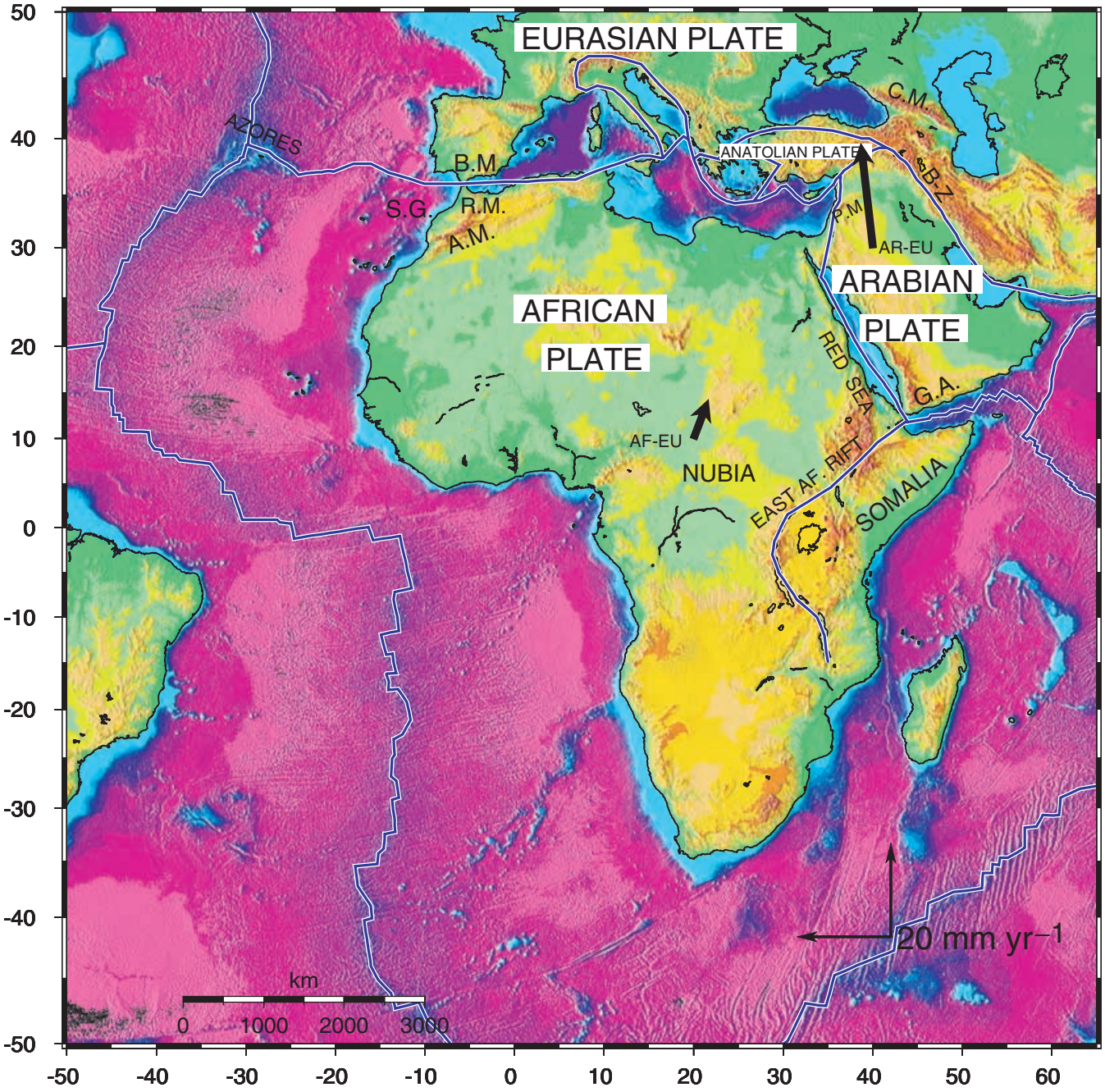

Figure 1. Topographic and bathymetric map of the African (Nubia–Somalia), Arabian and SW Eurasian plates showing schematic plate boundaries used in this study. Black arrows show NUVEL-1A motion of Arabia and Nubia (AF) relative to Eurasia. Abbreviations: SG, Straits of Gibraltar; BM, Betic Mountains; RM, Rif Mountains; AM, Atlas Mountains, PM, Palmyride Mountains; CM, Caucasus Mountains; B-Z, Bitlis–Zagros fold and thrust belt; GA, Gulf of Aden.

structures accommodating relative motion between the Nubian and Arabian plates. However, a simple geometric connection between the Red Sea rift and DSF is complicated by possible motion of the Sinai block, presumably along the Gulf of Suez (e.g. Steckler *et al.* 1998), and possible internal deformation of the Arabian Plate, most notably in the Palmyride fold and thrust belt (Chaimov *et al.* 1990).

During the Middle to Late Miocene (∼10 Ma), the Neo-Tethys closed between Arabia and Eurasia along the Bitlis suture in SE Turkey and the Bitlis–Zagros fold and thrust belt in Iran, initiating active continental collision (e.g. Sengor *et al.* 1985). Active deformation and associated crustal uplift in eastern Turkey, and shortening and mountain building in the Caucasus and Zagros have been attributed to this on-going continental collision (e.g. Sengor *et al.* 1985; Philip *et al.* 1989). Around 5 Ma, the East and North Anatolian faults were initiated and began accommodating the westward motion of the Anatolian Plate (e.g. Sengor 1979; Westaway 1994; Armijo *et al.* 1999).

The oceanic crust within the eastern Mediterranean basin is a remnant of the Neo-Tethys caught in the impending Nubia–Eurasia continental collision. It is being actively subducted along the Hellenic and Cyprus trenches, and presumably within the complexly deformed region connecting these trenches (although less well

defined) (e.g. Le Pichon & Angelier 1979; Klemper & Ben-Avraham 1987; Papazachos & Papaioannou 1999). Active subduction is also occurring southwest of Italy along the Calabrian trench. Migration of the Hellenic and Calabrian trenches over the subducting oceanic plate, presumably associated with foundering of the subducted lithosphere (Le Pichon & Angelier 1979; Royden 1993; Malverno & Ryan 1986; Jolivet & Faccenna 2000; Savelli 2002) has produced the Aegean and Tyrrhenian basins. Slab detachment and lithospheric delamination have also been proposed as influencing the character of surface deformation in the Mediterranean (e.g. Seber *et al.* 1996; Wortel & Spakman 2000).

The African 'plate' consists of two separate plates divided along the East African rift system, Nubia to the west and Somalia to the east. Extension across the rift, averaged over the past 3 Myr, has been estimated from an analysis of rates of sea-floor spreading to vary from (0–6) $\pm$ 1.5 mm yr^{-1} from south to north within the African continent (Chu & Gordon 1999).

The western Mediterranean has accommodated approximately 150–170 km of plate convergence since the Oligocene ($\sim$40 Ma). The current configuration, and geologically recent (i.e. Post to Early Miocene; $\sim$20 Ma) history of the African–Eurasian boundary in the western Mediterranean is complex, involving juxtaposed compression (Betic and Rif Mountains, Atlas Mountains) and extension (Alboran sea) (e.g. Dewey *et al.* 1989; Gomez *et al.* 2000). Further west in the Atlantic Ocean, the boundary is predominantly an oceanic transform fault that connects with the Mid-Atlantic Ridge near the Azores. The transform is complex involving distributed deformation, compression along the eastern segment, predominantly right-lateral, strike slip along the central segment and extension on the westernmost segment near the Azores (e.g. Udias *et al.* 1976; Buforn *et al.* 1988; Chen & Grimison 1989).

The most recent, geologically determined plate motions in the Mediterranean region (i.e. 3 Myr) are described by Euler vectors derived from analyses of sea-floor magnetic anomalies, transform fault orientations and global circuit closure (e.g. DeMets *et al.* 1990, 1994; Jestin *et al.* 1994; Chu & Gordon 1998). Estimates of present-day Euler vectors have been reported from an analysis of geodetic data by Larson *et al.* (1997) and Sella *et al.* (2002). Present-day plate motions have been estimated for smaller plates and blocks in the interplate deformation zone from seismic and neotectonic observations, analysis of satellite images (e.g. McKenzie 1972; Le Pichon & Angelier 1979; Jackson & McKenzie 1988) and from an analysis of geodetic data (e.g. Le Pichon *et al.* 1995; Robins *et al.* 1995; Reilinger *et al.* 1997; McClusky *et al.* 2000).

In this paper we use GPS observations to constrain present-day relative motion between Nubia, Arabia and Eurasia. We use the GPS-derived motions to determine relative Euler vectors for these plates and to compare them with Euler vectors determined from global and regional plate motion models and prior geodetic studies. We include motions of intervening plates/blocks (i.e. Anatolia and Aegea) determined previously by McClusky *et al.* (2000) and present the resulting sense and rate of deformation across plate boundaries. We consider the implications of the new, instantaneous Euler vectors for the rigidity of continental lithosphere, and possible temporal variations in plate motions.

GPS DATA ANALYSIS AND EULER VECTORS

The main data used for this study were continuous GPS data (CGPS) acquired by the International GPS Service (IGS) between 1992 and 2002. To improve station coverage on the African, Arabian, Anatolian and Aegean plates we also include five eastern Mediterranean (EMED) survey mode (SGPS) campaigns measured between 1992 and 2000 (McClusky *et al.* 2000). Fig. 2 shows, and Table 1 summarizes the station velocities in a Eurasia-fixed reference frame used to constrain Africa (Nubia), Arabia and Eurasia plate motions.

We analyse the data using the GAMIT/GLOBK software (Herring 1999; King & Bock 1999) in a two-step approach (e.g. Dong *et al.* 1998). In the first step, we use GPS phase observations from each day to estimate station coordinates, the zenith delay of the atmosphere at each station, and orbital and Earth orientation parameters (EOP). In the second step we use the loosely constrained estimates of station coordinates, orbits and EOP, and their covariances from each day, aggregated by survey, as quasi-observations in a Kalman filter to estimate a consistent set of coordinates and velocities. We provide orbital control and tie the regional EMED measurements to an external global reference frame by including in the regional analysis data from three to five continuously operating IGS stations for each day. The regional quasi-observations are then combined with quasi-observations from an analysis of phase data from over 100 stations performed by the Scripps Orbital and Permanent Array Center (SOPAC) at UC San Diego (Bock *et al.* 1997). Before estimating velocities in the second step of our analysis, we examine the time-series of position estimates to determine the appropriate weights to be applied to the surveys of each group. For the velocity solution, we reweight the quasi-observations such that the normalized long-term scatter in horizontal position for each group is unity. Finally, to account for correlated errors, we add to the assumed error in horizontal position a random walk component of 2 mm yr$^{-1/2}$ (McClusky *et al.* 2000).

The GPS-Euler vectors determined in this study and their 1σ uncertainties are given in Table 2 and their locations are shown in Figs 3 and 4 along with prior results from other studies (also listed and referenced in Table 2). The residual velocities (observed minus calculated; i.e. the component of the relative velocities not accounted for by the derived Euler vectors) are also shown in these figures. Euler vectors were estimated in a simultaneous least-squares solution, using the velocity solution and its full variance covariance matrix. The vector estimates are based on 23 stations located on the Eurasian Plate, eight on the Nubian Plate and four on the Arabian Plate (Table 1).

The Nubia–Eurasia GPS Euler vector provides a very good fit to well-constrained velocities [weighted root mean square (WRMS) residuals = 0.6 mm yr^{-1} for Nubia and Eurasia] at GPS stations widely distributed around the Nubian Plate (Fig. 3), providing strong constraints on the Euler vector (Fig. 3, and Table 2). This observation also demonstrates the coherent motion of the Nubian Plate with internal deformation constrained well below 1 mm yr^{-1} (1σ), at least on a plate-wide basis (i.e. more local deformation that does not effect overall plate coherence cannot be ruled out).

In contrast, the Arabia–Eurasia Euler vector (and consequently the Arabia–Africa Euler vector) is derived from only four GPS velocities (BAHR, KIZ2, GAZI, KRCD). Furthermore, sites in SE Turkey (KRCD, KIZ2, GAZI) lie near the Bitlis suture and East Anatolian fault (EAF), the boundary between the Anatolian and Arabian plates (Fig. 4). While we believe that these stations are well outside the elastic strain field (i.e. GAZI is approximately 90 km from the mapped surface trace of the EAF and KIZ2 is approximately 150 km from the Bitlis suture), faulting is complex and we cannot completely rule out some influence from plate boundary effects.

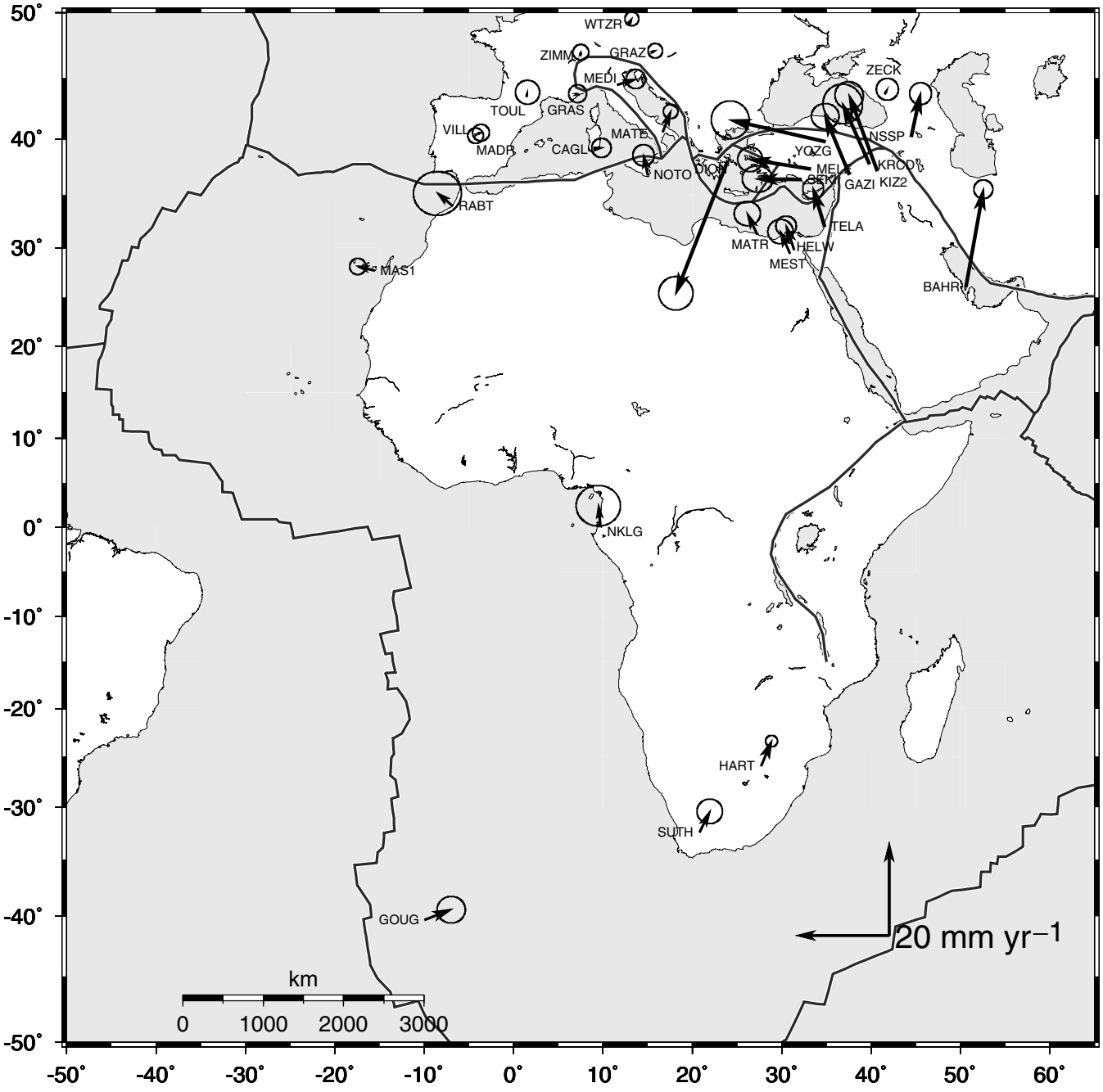

Figure 2. GPS velocities and 95 per cent confidence ellipses in a Eurasia fixed frame used to determine Nubia, Arabia and Eurasia relative Euler vectors. Not all GPS sites are shown on the Eurasian Plate. Selected GPS velocities within the eastern and central Mediterranean deforming zone (Anatolian, Aegean and Adriatic 'plates') are also shown. Plate boundaries are as in Fig. 1.

PRESENT-DAY MOTION ACROSS PLATE BOUNDARIES

As indicated in Fig. 3 and Table 2, there are significant differences between the well-determined GPS Nubia–Eurasia Euler vector and that reported from the NUVEL circuit closure model. The GPS Euler vector is derived from observations spanning approximately 10 yr, while the NUVEL result is based primarily on an analysis of magnetic anomalies and transform fault orientations and is reported as a 3 Myr average. The question arises as to whether the GPS result represents a change in plate motions during the past few million years. Sella *et al.* (2002) appeal to longer-term geological data that indicate a Miocene to present deceleration of spreading in the south Atlantic (Cante & Kent 1992) to suggest a possible explanation for slow geodetic motion of the African Plate compared with the 3 Myr NUVEL-1A result. However, DeMets *et al.* (1990, 1994) acknowledge the shortcomings of their model, which assumes a single African Plate (i.e. no allowance is made for separate Nubian and Somalian plates). Current estimates for spreading rates in the East African rift reach 6 ± 1.5 mm yr^{-1} near the northern end of the rift (Chu & Gordon 1999). These rates are similar to Africa–Eurasia relative plate motion rates. An accurate assessment

Table 1. GPS velocities in a Eurasia-fixed reference frame (as defined in this study), 1σ uncertainties ($\pm$), and correlation between the east and north components of velocity (RHO), used to estimate Euler vectors: * = Arabia, # = Eurasia, + = Africa. Velocities for other stations shown in the figures are also listed.

Long. (°E)	Lat. (°N)	E (mm yr^{-1})	N (mm yr^{-1})	E ($\pm$)	N ($\pm$)	RHO	Site
50.60	26.20	3.72	20.79	0.83	0.82	0.001	BAHR*
40.65	37.24	−5.97	16.09	1.24	1.21	−0.029	KIZ2*
39.80	37.84	−5.71	12.83	1.73	1.73	−0.019	KRCD*
37.57	36.90	−5.20	12.47	1.21	1.11	0.000	GAZI*
−3.95	40.44	0.59	0.26	0.74	0.73	0.000	VILL#
−4.25	40.42	0.00	−0.35	0.68	0.67	0.001	MADR#
36.75	55.69	−0.12	−0.63	0.76	0.75	0.000	ZWEN#
21.03	52.09	−0.04	0.21	0.71	0.71	−0.002	JOZE#
18.93	69.66	−1.02	0.69	0.65	0.65	−0.001	TROM#
17.07	52.27	0.26	0.21	0.75	0.75	−0.001	BOR1#
15.49	47.06	0.68	0.29	0.64	0.64	0.000	GRAZ#
13.06	52.37	0.45	0.23	0.76	0.75	−0.001	POTS#
12.87	49.14	0.66	0.90	0.61	0.61	−0.001	WTZR#
11.92	57.39	−1.02	−0.55	0.62	0.62	0.000	ONSA#
24.39	60.21	0.23	−0.67	0.67	0.66	−0.001	METS#
104.31	52.21	−1.10	−0.46	0.79	0.78	−0.005	IRKT#
92.79	55.99	−0.86	0.04	1.02	0.99	−0.006	KSTU#
129.68	62.03	−0.77	0.37	0.89	0.88	0.000	YAKT#
58.56	56.43	−0.41	0.71	1.43	1.38	0.007	ARTU#
128.86	71.63	0.62	0.94	1.14	1.13	−0.001	TIXI#
1.48	43.56	0.15	0.92	1.06	1.05	0.000	TOUL#
11.86	78.93	0.09	−0.33	0.67	0.66	−0.001	NYAL#
7.46	46.87	0.11	0.51	0.69	0.68	−0.002	ZIMM#
6.92	43.75	0.46	0.10	0.78	0.78	−0.001	GRAS#
5.81	52.17	−0.04	0.20	0.62	0.62	−0.001	KOSG#
4.35	50.79	0.10	−0.48	0.73	0.73	−0.001	BRUS#
41.56	43.78	0.48	0.95	0.97	0.96	0.000	ZECK#
8.97	39.13	1.63	0.24	0.85	0.84	−0.003	CAGL
−9.88	−40.34	5.56	2.19	1.24	1.17	0.003	GOUG+
−15.63	27.76	−3.45	0.89	0.71	0.71	0.002	MAS1+
31.34	29.86	−1.65	5.03	0.90	0.86	0.000	HELW+
30.88	29.51	−1.97	4.57	1.11	1.07	−0.004	MEST+
27.70	−25.88	2.21	5.25	0.52	0.50	−0.003	HART+
27.23	31.34	−2.08	4.39	1.15	1.06	0.002	MATR+
20.81	−32.38	2.17	4.37	1.12	1.08	0.004	SUTH+
9.67	0.35	−0.37	3.99	1.94	1.78	−0.003	NKLG
−6.85	33.99	−3.19	2.71	2.10	1.93	0.010	RABT
14.99	36.87	−0.87	4.14	0.94	0.93	−0.001	NOTO
11.64	44.52	3.89	1.19	0.84	0.84	−0.003	MEDI
16.70	40.64	1.67	4.31	0.64	0.63	−0.002	MATE
44.50	40.22	1.97	9.18	0.96	0.96	−0.001	NSSP
34.78	32.06	−2.43	8.10	0.92	0.91	−0.001	TELA
33.39	35.14	−7.04	3.07	0.97	0.96	−0.002	NICO
23.93	38.07	−11.08	−28.37	1.50	1.47	−0.002	DION

of how including Nubian and Somalian plates in the NUVEL model will affect Nubia Plate motion estimates will require a complete reanalysis of the data that went into this model, an effort that is proceeding at the present time (DeMets, personal communication, 2002).

As indicated in Fig. 4 and Table 2, there are significant differences between the Nubia–Arabia GPS and NUVEL Euler vectors. In contrast, the more recent Nubia–Arabia Euler vector determined by Chu & Gordon (1998) from magnetic anomalies in the Red Sea (and hence a 3 Myr average such as NUVEL) agrees within confidence intervals with the GPS determination with regard to the pole location and rotation rate. Given the acknowledged limitations of the NUVEL global solution, this agreement indicates no significant change in motion of the Arabian Plate with respect to Nubia during the past 3 Myr, at least at the level of detection of the current data ($\sim$1 mm yr^{-1}). Ongoing and expanding efforts to monitor with GPS present motions of the Arabian Plate should provide tighter constraints on the GPS Nubia–Arabia Euler vector, allowing more definitive conclusions concerning possible temporal changes in Arabia Plate motion.

Relative motion derived from the GPS-Euler vectors across simplified plate boundaries (Figs 4, 5a and 6a), and earthquake focal mechanisms for large ($M > 6.0$), shallow (<50 km), and historic earthquakes (Figs 5b and 6b) (Harvard catalogue and others; see McClusky *et al.* 2000, for references), provide the opportunity to examine plate interactions. The plate boundaries we show in these figures are highly schematic, particularly those located within the continental lithosphere. Interplate deformation is, in at least some

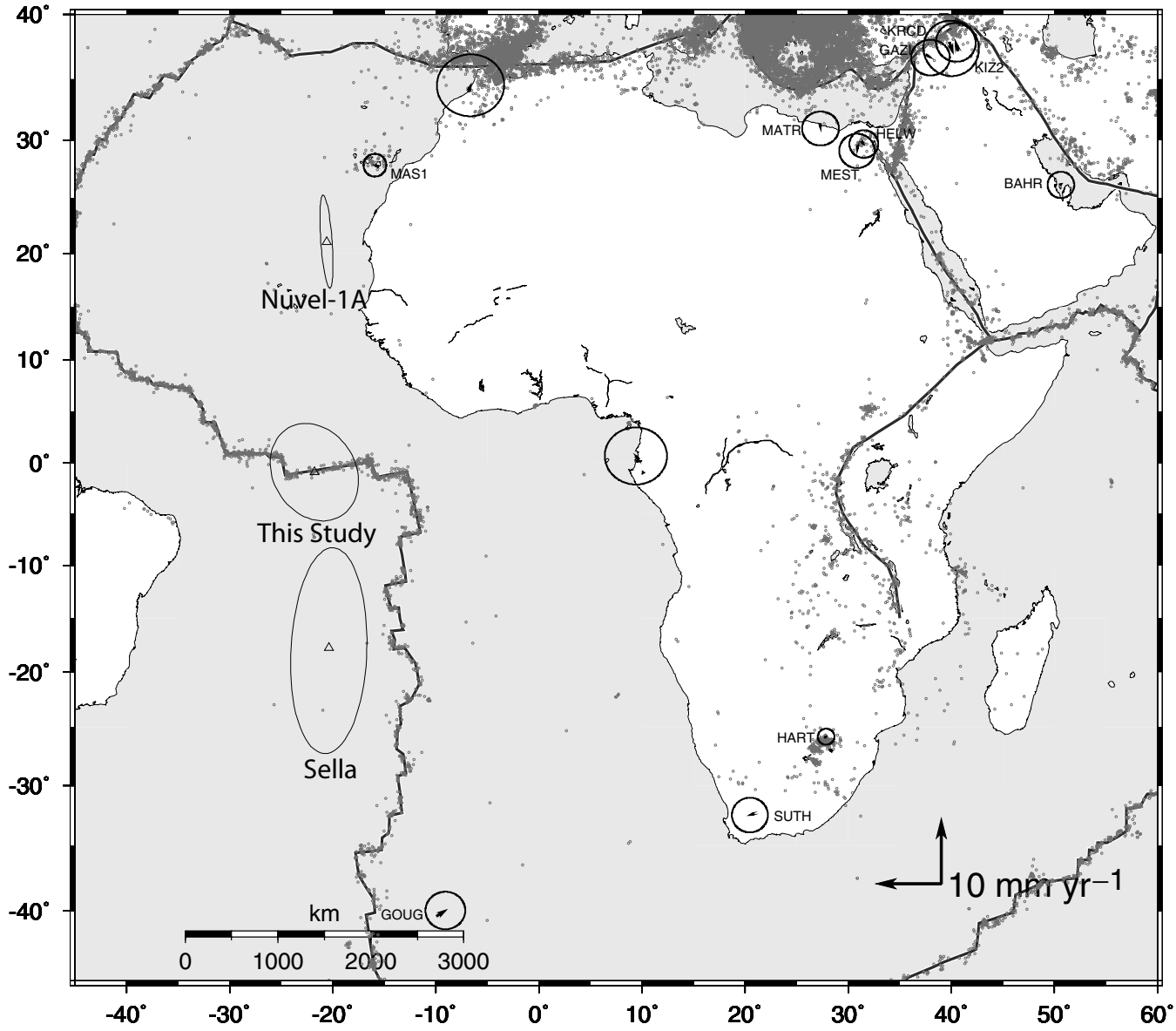

Figure 3. Nubia–Eurasia Euler poles and 1σ uncertainties (see Table 2). GPS station residuals and 95 per cent confidence ellipses are also shown. Residuals for stations on the Arabia Plate are from the Arabia–Eurasia Euler vector (see Table 2 and Fig. 4). Sites with names (four-character ID) were used to estimate the Euler vectors for Arabia and Nubia. Seismicity (depths <33 km) (http://www.seismology.harvard.edu), and schematic plate boundaries are also shown (plate boundaries are as in Fig. 1). The WRMS GPS velocity residuals for Nubia, Arabia and Eurasia are 0.6, 0.8 and 0.6 mm yr^{-1}, respectively.

cases, distributed across a number of tectonic structures within the boundary zone. However, we believe the relative motions shown in Figs 4, 5(a) and 6(a) provide improved boundary conditions for more detailed studies of plate interactions (i.e. the overall motion that must be accommodated across the plate boundary zone).

The schematic Arabia–Eurasia plate boundary corresponds to the Bitlis suture and East Anatolian fault in SE Turkey and the main recent fault and Bitlis–Zagros fold and thrust belt in Iran. While part of Arabia–Eurasia convergence is accommodated in the Caucasus and northern Iran, we do not include these structures in our plate model since data available for this study do not constrain the partitioning of deformation across this area. The Nubia–Arabia boundary is well determined in the Red Sea (Chu & Gordon 1998), and along the DSF (Joffe & Garfunkel 1987), although more detailed studies indicate local complexities (e.g. Butler *et al.* 1997; Chu & Gordon 1998; Gomez *et al.* 2001). Similarly, the general location of the subduction/transform boundaries along the Cyprus and Hellenic trenches, and to a lesser extent, the Florence rise, are reasonably well known and are well defined by narrow bands of seismicity (at least for the Hellenic and Cyprus trenches) and well imaged down-going lithosphere (e.g. Wortel & Spakman 2000). However, along the Cyprus trench and Florence rise, the Nubian Plate interacts with the Anatolian Plate and along the Hellenic trench with the Aegean Plate (McKenzie 1972; McClusky *et al.* 2000). Accordingly, we use the Euler vectors derived by McClusky *et al.* (2000) for Anatolia and Aegea to estimate orientations and rates of relative motion on these boundaries (Table 2). Various models have been proposed for the plate boundary in the central Mediterranean where seismicity is more diffuse (e.g. Savelli 2002, and references therein). As indicated in Fig. 6(a) (i.e. large GPS residual motions relative to Eurasia), the eastern part of the Italian Peninsula is clearly not part of the Nubian or Eurasian plates and a single boundary separating

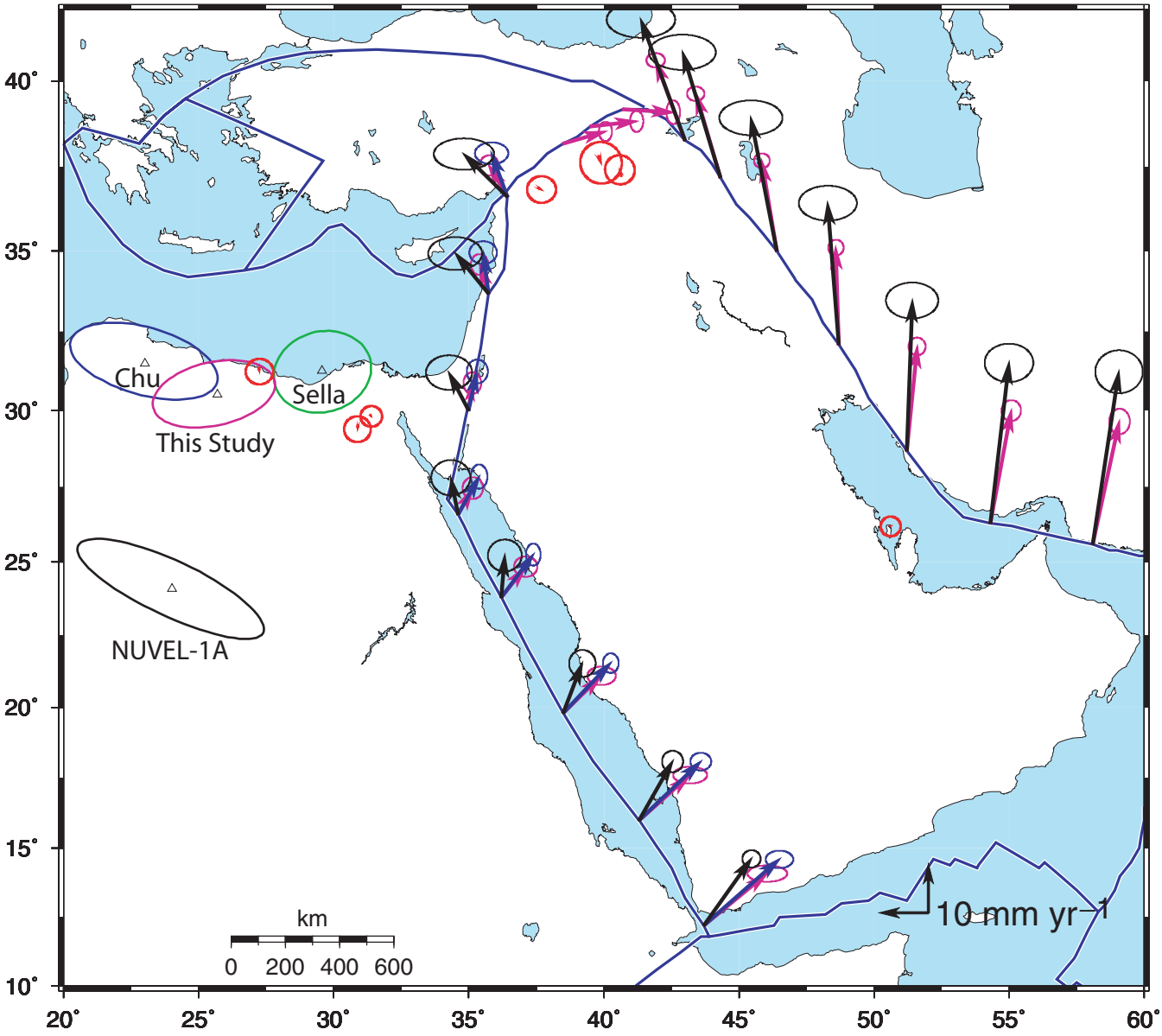

Figure 4. GPS (this study, in red), NUVEL-1A (black), Chu & Gordon (1998) (blue), and Sella *et al.* (2002) (green) Euler poles and 1σ uncertainties, and predicted motions along the boundary of the Arabian Plate (for clarity, we do not show the Sella *et al.* predicted motions that differ insignificantly from those determined in this study). Motions are for Arabia relative to the adjacent plate. Residual velocities and 95 per cent confidence ellipses for Arabia and Nubia (red) are also shown. Note close agreement in orientation of relative plate motions as determined by the Chu & Gordon (1998) 3 Myr average and those determined in this study. While the GPS relative motions are less than those determined by Chu and Gordon, the difference is not significant at the 95 per cent confidence level. Schematic plate boundaries are as in Fig. 1.

Nubia and Eurasia in the central Mediterranean is overly simplistic. Because we have little quantitative information on block motions in the Adriatic (e.g. Nocquet *et al.* 2001), we ignore these complications for now and show only Nubia–Eurasia motion along a boundary south of the Italian peninsula. Moving westward, we locate the Nubia–Eurasia boundary along the Calabrian trench, ignoring possible extension within the backarc. Seismicity, and hence the location of the plate boundary (or boundaries) remains diffuse through the western Mediterranean to the straights of Gibraltar. From there, the boundary is reasonably well defined to the Mid-Atlantic ridge, although it is diffuse west of Gibraltar and near the Azores.

As indicated in Fig. 4, the GPS result agrees very well with the orientation of relative motion predicted by the Chu & Gordon (1998) Arabia–Nubia Euler vector along the Red Sea and DSF. The GPS motions are smaller than the geological result, but the difference is within the uncertainties. The GPS result implies spreading rates along the Red Sea varying from 14 ± 1 mm yr^{-1} at 15°N to 5.6 ± 1 mm yr^{-1} at 27°N. The GPS Euler vector indicates left-lateral strike-slip motion along the DSF in the Gulf of Aqaba, with increasing compression towards the north. Rates of motion also increase to the north along the DSF from 5.6 ± 1 mm yr^{-1} of pure left-lateral strike slip on the southernmost DSF to 7.5 ± 1 mm yr^{-1} near the DSF–EAF junction. Along the northern DSF (i.e. north of the Lebanon restraining bend) motion is partitioned between 6 ± 1 mm yr^{-1} fault parallel and 4 ± 1 mm yr^{-1} fault normal motion. The GPS results indicate compression along the southernmost Zagros (∼26°N) at 23 ± 1 mm yr^{-1}, with decreasing amplitude and an increasing component of right-lateral strike-slip motion to the north

Table 2. GPS-Euler vectors and 1σ uncertainties (EU = Eurasia, AN = Anatolia, AE = Aegea, AR = Arabia, AF = Africa, NU = Nubia, * = new result from this study).

Plates	Lat. (°N)	Long (°E)	Rate (deg Myr^{-1})	Ref.
*EU–NU	-0.95 ± 4.8	-21.8 ± 4.3	0.06 ± 0.005	This study
EU–NU	-18.23 ± 9.5	-20.01 ± 3.7	0.062 ± 0.005	Sella *et al.* (2002)
EU–AF	21.0 ± 4.2	-20.6 ± 0.6	0.12 ± 0.015	DeMets *et al.* (1994)
*AR–EU	27.4 ± 1.0	18.4 ± 2.5	0.40 ± 0.04	This study
AR–EU	25.6 ± 2.1	19.7 ± 4.1	0.5 ± 0.1	McClusky *et al.* (2000)
AR–EU	24.6 ± 1.6	13.7 ± 3.9	0.5 ± 0.05	DeMets *et al.* (1994)
AR–EU	26.22 ± 2.1	22.87 ± 1.1	0.427 ± 0.029	Sella *et al.* (2002)
*AR–NU	30.5 ± 1.0	25.7 ± 2.3	0.37 ± 0.04	This study
AR–NU	31.26 ± 1.3	29.55 ± 1.8	0.400 ± 0.030	Sella *et al.* (2002)
AR–NU	32.59	23.70	0.418	Jestin *et al.* (1994)
AR–NU	31.5 ± 1.2	23.0 ± 2.7	0.40 ± 0.05	Chu & Gordon (1998)
AR–NU	32.2	24	0.376	Joffe & Garfunkel (1987)
AR–AF	24.1 ± 1.7	24.0 ± 3.5	0.40 ± 0.05	DeMets *et al.* (1994)
AN–EU	30.7 ± 0.8	32.6 ± 0.4	1.2 ± 0.1	McClusky *et al.* (2000)
AN–EU	14.6	34	0.64	Jackson & McKenzie (1984)
AN–EU	14.6	34	0.78	Taymaz *et al.* (1991)
AN–EU	31	35.5	0.83 ± 0.1	Westaway (1994)
AN–EU	30	34	0.44	Le Pichon & Angelier (1979)
AN–EU	32.73	32.03	1.72	Le Pichon *et al.* (1995)
AN–AR	32.9 ± 1.3	40.3 ± 1.3	0.8 ± 0.2	McClusky *et al.* (2000)
AN–AR	−20.6	68.9	0.34	Jackson & McKenzie (1984)
AN–AR	−3.3	61.9	0.35	Taymaz *et al.* (1991)
AE–AN	38.0 ± 0.5	19.6 ± 1.2	1.2 ± 0.2	McClusky *et al.* (2000)

(19 ± 1 mm yr^{-1} at an angle of approximately 30° to the main structural trend of the mountain range at 35°N), although this motion is partitioned across other structures further north of this schematic boundary (e.g. Reilinger *et al.* 1997; McClusky *et al.* 2000; Tatar *et al.* 2002).

Fig. 5(a) shows relative motions along the boundaries of the Anatolian and Aegean plates, where Anatolian and Aegean plate motions are determined from results presented by McClusky *et al.* (2000) (see Table 2 for Euler vectors). Along the EAF (Arabia–Anatolia) motions are predominantly left-lateral, strike slip at 9 ± 1 mm yr^{-1}. There is a component of extension, particularly along the eastern segment of the fault west of the Karliova Triple Junction. The eastern segment of the Cyprus trench is characterized by left-lateral motion with increasing tension towards the east (i.e. Gulf of Iskenderum, near the junction of the DSF, EAF), consistent with the tensional focal mechanisms around the Gulf (Fig. 5b). To the west, the Cyprus and Hellenic trenches are dominated by compression with a large component of left-lateral motion along the Plino–Strabo trench. The Aegean Plate is moving rapidly towards the SW relative to surrounding plates (30 ± 1 mm yr^{-1} relative to Eurasia), giving rise to extension in western Turkey ($10–15 \pm 1$ mm yr^{-1}), and in the Gulf of Corinth/central Greece ($\sim 30 \pm 1$ mm yr^{-1}), although how 'extension' is accommodated in central Greece remains enigmatic (Goldsworthy *et al.* 2002). The North Anatolian fault (Anatolia–Eurasia) is dominated by right-lateral strike slip (24 ± 1 mm yr^{-1}) with slight compression along the easternmost segment and extension in the Marmara Sea–North Aegean trough. Apart from the Cyprus trench—Florence Rise where seismicity rates are low (as are relative motions), these general patterns are in good agreement with the focal mechanisms shown in Fig. 5(b).

In the central and western Mediterranean (Figs 6a and b) a simple Nubia–Eurasia boundary is insufficient to account for the well-determined motions of IGS stations MATE and MEDI in Italy. Clearly, the Italian peninsula and Adriatic are not part of either the Eurasian or Nubian plates. In contrast, the motion of at least the southern part of Sicily (NOTO; 4.2 ± 1.2 mm yr^{-1} NW) is consistent with Nubia motion (Nubia–Eurasia motion north of NOTO is 5 ± 1 mm yr^{-1} NW), suggesting that the Nubia–Eurasia boundary lies north of station NOTO and south of Sardinia (i.e. CAGL displays Eurasia motion). West of Sicily, seismicity is mostly confined to the coastal region of N. Africa. Here, the GPS relative motions indicate right-lateral, strike slip and compression across the assumed, simple boundary with total relative motion of 5 ± 1 mm yr^{-1}. This sense of relative motion is qualitatively consistent with the focal mechanism solutions (Fig. 6b). In the westernmost Mediterranean (Gibraltar, Alboran Sea), relative motions become increasingly right-lateral strike slip. Station SFER in southernmost Spain shows motion more consistent with Nubia than Eurasia. In addition, focal mechanisms in northern Morocco and the Alboran Sea indicate a significant component of extension. This inconsistency between GPS relative motions and seismicity suggests that deformation is more complex than is implied by the simple boundary model used in our analysis, a conclusion supported by neotectonic studies (e.g. Seber *et al.* 1996; Gomez *et al.* 2000; Gutscher *et al.* 2002). West of Gibraltar, Nubia–Eurasia motion becomes less compressional and more right-lateral strike slip to 17°W, increasing compression to approximately 24°W, and a significant component of extension to the Mid-Atlantic Ridge (i.e. Azores). Relative rates of motion are roughly constant along the plate boundary in the Atlantic at approximately $4–5 \pm 1$ mm yr^{-1}. Although focal mechanisms are mostly confined to the Azores along the plate boundary in the Atlantic, those that are available agree qualitatively with the GPS relative motions.

IMPLICATIONS FOR CONTINENTAL DEFORMATION

It is clear form the geodetic data presented here that deformation within the zone of interaction of the Arabia, Nubia and Eurasia

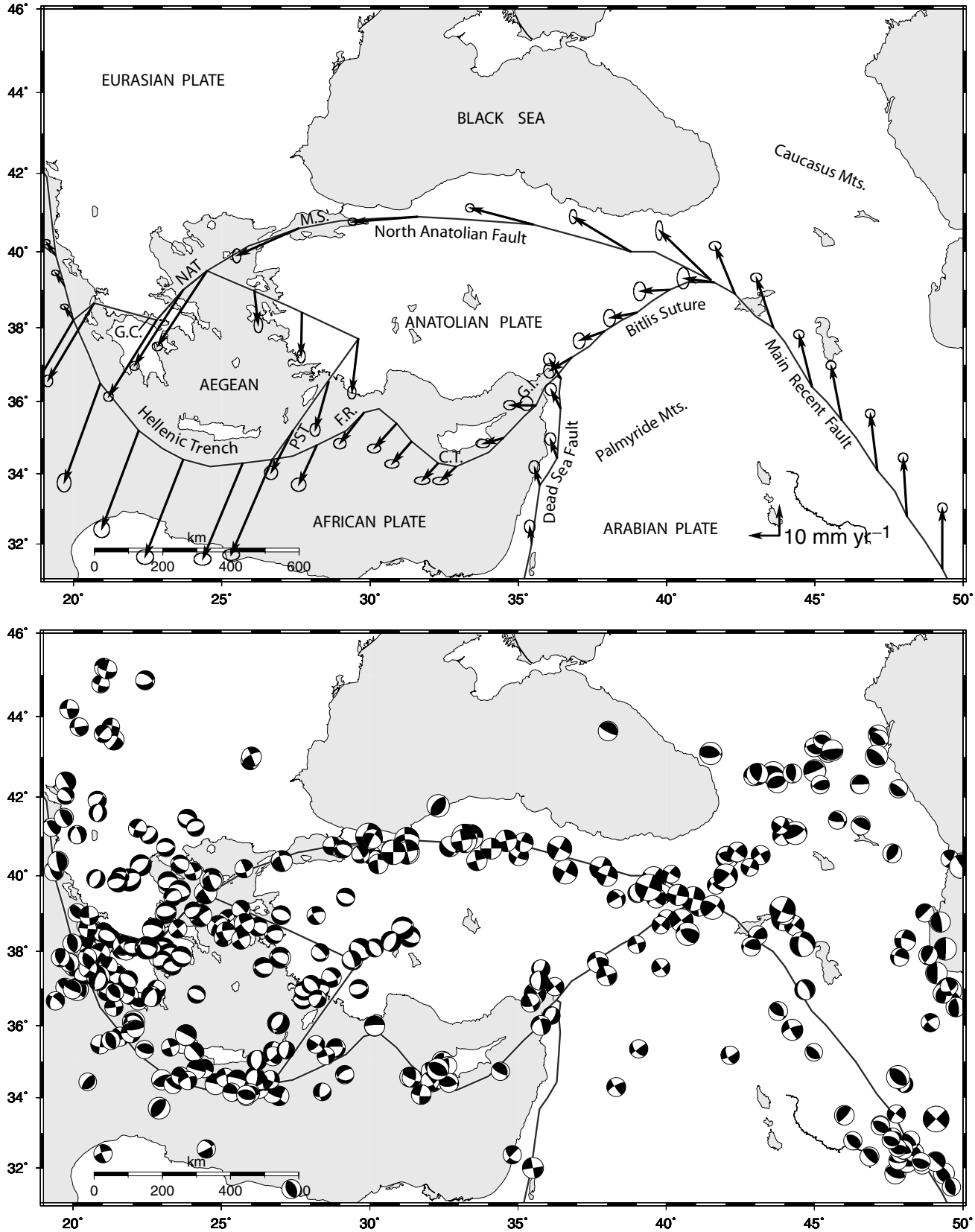

Figure 5. (a) Relative motions and 95 per cent confidence ellipses on schematic plate boundaries in the eastern Mediterranean derived from the Euler vectors determined in this study. Motions around the Arabian Plate are as in Fig. 4. Motions around the Aegean show Aegean motion relative to bordering plates. Motions along the boundaries of the Anatolian Plate show Anatolia motion relative to bordering plates, except where it is bordered by the Aegean Plate. Abbreviations: NAT, North Aegean Trough; MS, Marmara Sea; PST, Plino–Strabo Trench; FR, Florence Rise; GI, Gulf of Iskenderum. (b) Earthquake focal mechanisms (lower hemisphere projection) for large ($M > 6$), shallow (<50 km), earthquakes (http://www.seismology.harvard.edu/CMTsearch.html).

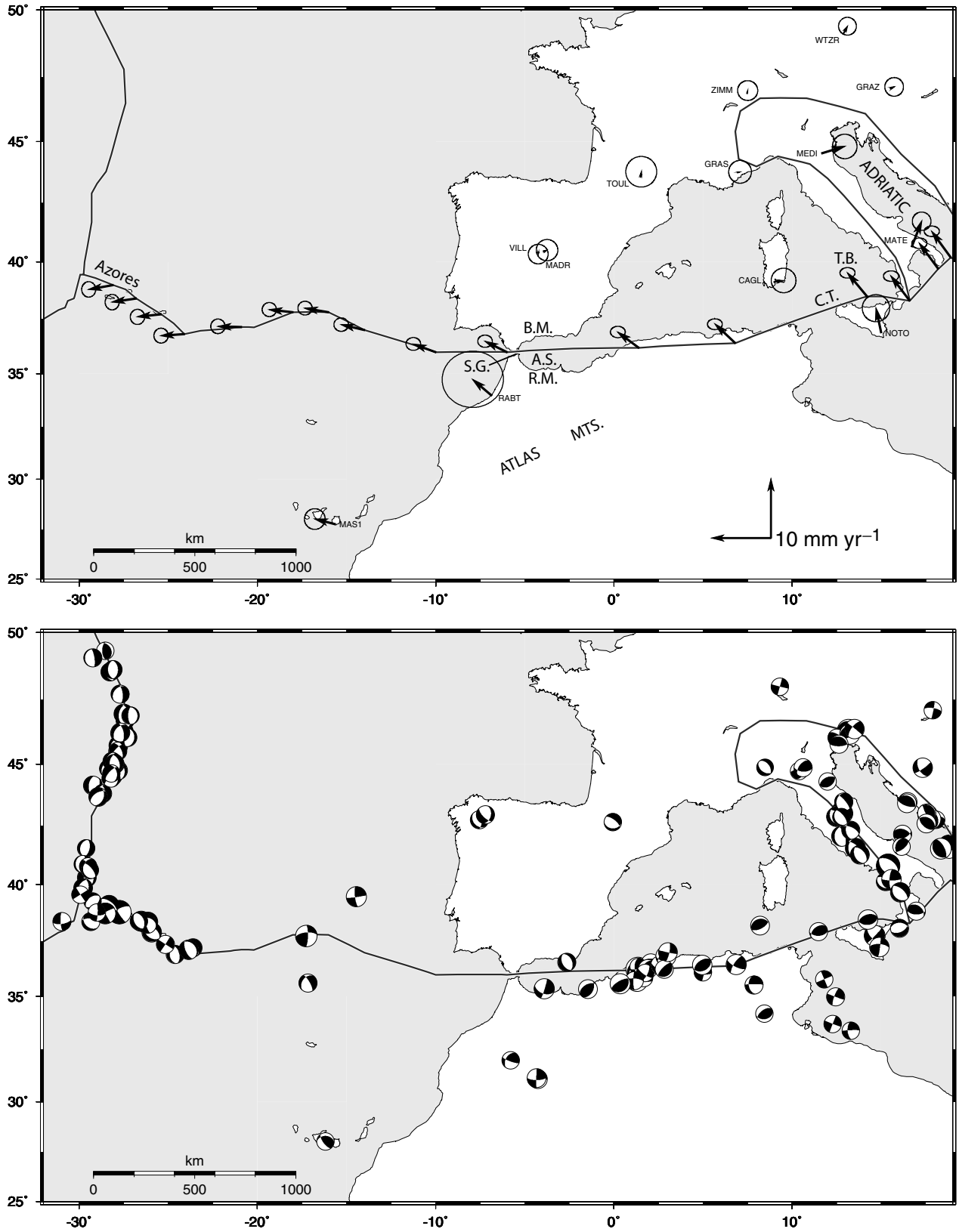

Figure 6. (a) Motions of Africa (Nubia) relative to Eurasia on schematic plate boundaries in the central, and western Mediterranean, and in the eastern Atlantic Ocean derived from the Euler vectors determined in this study. Selected GPS site velocities and 95 per cent confidence ellipses in a Eurasia-fixed reference frame are also shown. The GPS velocities at stations MEDI and MATE indicate that the eastern part of the Italian peninsula (Adriatic) is not part of either the Eurasian or African plate. Abbreviations: SG, Straits of Gibraltar; BM, Betic Mountains; AS, Alboran Sea; RM, Rif Mountains; CT, Calabrian Trench; TB, Tyrrhenian Basin. (b) Earthquake focal mechanisms (lower hemisphere projection) for large ($M > 6$), shallow (<50 km), earthquakes (http://www.seismology.harvard.edu/CMTsearch.html).

plates is complex involving intervening, smaller plates or blocks (e.g. Anatolian, Aegean, Adriadic, Alboran Sea). In some areas such as western Turkey, the Zagros of western Iran and central Greece, deformation appears to be more spatially diffuse as indicated by dense geodetic observations, the distribution of seismic activity, active faulting and mountain building (e.g. Jackson *et al.* 1995; Davies *et al.* 1997; Tatar *et al.* 2002). On the other hand, more spatially dense geodetic observations for a substantial part of the eastern Mediterranean region and the distribution of historic earthquakes are at least compatible with relatively simple models involving a small number of plates or blocks with the bulk of the deformation confined to narrow block/plate boundaries (e.g. Armijo *et al.* 1996; Kahle *et al.* 2000; McClusky *et al.* 2000; Nocquet *et al.* 2001; Meade *et al.* 2002). Debate continues as to whether plate/block or continuum descriptions (or some combination) represent better the behaviour of active deformation within the continental lithosphere of the Mediterranean region (e.g. Jackson *et al.* 1995; Thatcher 1995; Davies *et al.* 1997; Armijo *et al.* 1999; McClusky *et al.* 2000).

As demonstrated in this paper, it is possible to determine reference frames in which the large majority of relative site motions can be reduced to insignificance for the 'interior' (i.e. away from broad active boundaries) of the Nubian, Eurasian and Arabian plates. The geodetic result for Arabia is tentative due to limited spatial coverage, however, the agreement between the geodetic and geological (i.e. Red Sea magnetic anomalies) Euler vectors suggests that further data will only strengthen this conclusion. This alone would appear to validate the utility of a plate description of contemporary deformation. However, a further test of the utility of this approach is to compare the slip rates on plate bounding faults derived from the relative Euler vectors with those determined from near-fault geodetic studies and neotectonic evidence. Sufficient data are available to do this for the North Anatolian fault (Anatolian–Eurasia boundary), East Anatolian fault (Arabian–Anatolian boundary) and the Dead Sea fault/Red Sea rift (Arabian–Nubian plate boundary).

The GPS Anatolia–Eurasia Euler vector predicts slip rates at the location of the NAF of 24 $\pm$ 1 mm yr^{-1}. Slip rates for the NAF are reported from near-field GPS studies and neotectonic studies of fault offsets and ages. Meade *et al.* (2002) report a rate of 25.6 $\pm$ 0.7 mm yr^{-1} based on the most recent GPS data around the western segment of the NAF fault. This agreement indicates that all relative plate motion, within the measurement uncertainty, is accommodated along the fault, at least along the segment where sufficiently dense GPS data allow a local determination.

McClusky *et al.* (2000) review geological evidence for NAF slip rates based primarily on the total offset and age of the fault. These estimates vary widely (16–25 mm yr^{-1}) and are not particularly useful at this stage for comparing with predicted rates from plate motion models.

The Anatolian–Arabian Euler vector predicts 9 $\pm$ 1 mm yr^{-1} left-lateral motion on the EAF. At present, insufficient geodetic data are available in the near field of the EAF to constrain fault characteristics (slip rates and locking depths). Geological estimates have been reported in the range 4–7 mm yr^{-1} (e.g. Arpat & Saroglu 1972; Dewey *et al.* 1986), somewhat smaller than the plate motion estimate. This apparent discrepancy may reflect off-fault deformation, a possibility supported by neotectonic studies (e.g. Westaway 1994). However, the significance of this apparent difference remains uncertain given the difficulty of dating fault offsets, and possible missed offsets on parallel structures.

The Nubia–Arabia GPS Euler vector predicts 5.8 $\pm$ 1 mm yr^{-1} left-lateral slip on the southern Dead Sea fault in Israel. This rate is slightly higher than that determined by regional geodetic studies confined primarily to the western side of the fault (Pe'eri *et al.* 2002, 2.6 $\pm$ 1.1 mm yr^{-1}) but does not differ significantly from geomorphological studies of the DSF in Israel (Klinger *et al.* 2000, 4 $\pm$ 2 mm yr^{-1} since the Late Pleistocene). The possibly higher DSF rate we determine in comparison with regional GPS studies could reflect active opening of the Gulf of Suez rift estimated at $\sim$1 mm yr^{-1} (Steckler *et al.* 1998), but the GPS data are not yet sufficient to justify this conclusion. As stated earlier, there is no significant difference between rates of rifting in the Red Sea as determined from analysis of marine magnetic anomalies (i.e. localized spreading along the rift axis) and those derived from overall, present-day plate motions. Although uncertainties are high ($\sim$25 per cent or more of the total slip rates) these observations provide no support for substantial off-fault or internal plate/block deformation within the continental lithosphere of the Nubian, Eurasian or Arabian plates.

CONCLUSIONS

We present a well-constrained Nubia–Eurasia GPS Euler vector that differs significantly from the NUVEL-1A, 3 Myr average. Because of the well-known limitations in the NUVEL result, it is not yet possible to determine whether this difference is due to systematic errors or changes in plate motion rates over the past 3 Myr. We also present a preliminary Arabia–Eurasia (and Arabia–Nubia) GPS Euler vector that differs from the NUVEL-1A result, but is statistically consistent with the updated 3 Myr geological Euler vector reported by Chu & Gordon (1998). These new GPS Euler vectors, listed in Table 2, are the principal results of this study.

We resolve no significant internal deformation of the Nubian Plate as a whole. The WRMS misfit to a coherent plate motion model is 0.6 mm yr^{-1}, below the resolution of the GPS data. The Nubia–Eurasia Euler vector lies approximately 20° south of the NUVEL-1A result. The Nubia–Eurasia GPS Euler vector implies NW–SE convergence within the Mediterranean with a substantially larger west component of motion for Nubia along the plate boundary zone than the NUVEL result. In addition, there is little variation in rates of motion along the boundary, ranging from 5.4 $\pm$ 1 mm yr^{-1} in the eastern Mediterranean to 4.5 $\pm$ 1 mm yr^{-1} near Gibraltar.

We use a simple plate boundary model to investigate deformation within the plate boundary zones. While this model is greatly oversimplified, it allows investigation of the total deformation that is being accommodated within these areas and as such provides overall 'boundary conditions' for more detailed models. The largest relative motions across plate boundaries occur along the Hellenic trench (35 $\pm$ 1 mm yr^{-1}), within the Gulf of Corinth and central Greece ($\sim$30 $\pm$ 1 mm yr^{-1}), along the North Anatolian fault 24 $\pm$ 1 mm yr^{-1}), and along the Zagros fold and thrust belt and associated deformation zones to the northeast (19–23 $\pm$ 1 mm yr^{-1}). These structures also display the highest seismic energy release. Slip rates on the DSF vary from pure left-lateral strike slip along the Gulf of Aqaba and southernmost DSF segment (5.6 $\pm$ 1 mm yr^{-1}) to left-lateral transpression with 6 $\pm$ 1 mm yr^{-1} strike-slip and 4 $\pm$ 1 mm yr^{-1} compression along the northern DSF in Syria. Overall, there is good, qualitative agreement between the sense of motion indicated by the GPS Euler vectors and earthquake focal mechanisms.

ACKNOWLEDGMENTS

We are indebted to the many individuals who established and maintained the IGS GPS stations that provided much of the data used in this study, and the SOPAC Data and Analysis Center that made these data available. We thank Chuck DeMets for providing us with

a copy of his software to calculate NUVEL-1A plate motion rates, and Giovanni Sella for providing us with a preprint of his paper on plate motions. Michael Steckler and James Cochran provided helpful discussions on the geological evolution of the Red Sea region. The maps in this paper were produced using the public domain Generic Mapping Tools (GMT) software (Wessel & Smith 1995). This research was supported in part by NSF Grants EAR-9814964, EAR-9909730, INT-0001583 and NASA grant NAG-9057.

REFERENCES

Armijo, R., Meyer, B., King, G.C.P., Rigo, A. & Papanastassiou, D., 1996. Quaternary evolution of the Corinth Rift and its implications for the Late Cenozoic evolution of the Aegean, *Geophys. J. Int.,* **126,** 11–53.

Armijo, R., Meyers, B., Hubert, A. & Barka, A., 1999. Propagation of the North Anatolian fault into the northern Aegean: timing and kinematics, *Geology,* **27,** 11–53.

Arpat, E. & Saroglu, F., 1972. The East Anatolian fault system: thoughts on its development, *Bull. Min. Res. Explor. Inst. Turkey,* **78,** 33–39.

Bock, Y., Behr, J., Fang, P., Dean, J. & Leigh, R., 1997. Scripps Orbit and Permanent Array Center (SOPAC) and Southern California Permanent GPS Array (PGGA), in *The Global Positioning System for the Geosciences,* pp. 55–61, Nat. Acad. Press, Washington, DC.

Buforn, E., Udias, A. & Colombas, M.A., 1988. Seismicity, source mechanisms and tectonics of the Azores–Gibraltar plate boundary, *Tectonophysics,* **152,** 89–118.

Butler, R.W.H., Spencer, S. & Griffiths, H.M., 1997. Transcurrent fault activity on the Dead Sea Transform in Lebanon and its implications for plate tectonics and seismic hazard, *J. geol. Soc. Lond.,* **154,** 757–760.

Cante, S.C. & Kent, D.V., 1992. A new geomagnetic polarity time scale for the Late Cretaceous and Cenozoic, *J. geophys. Res.,* **97,** 13 917–13 951.

Chaimov, T.A., Barazangi, M., Al-Saad, D., Sawaf, T. & Gebran, A., 1990. Crustal shortening in the Palmyride fold belt, Syria, and implications for movement along the Dead Sea fault system, *Tectonics,* **9,** 1369–1386.

Chen, W. & Grimison, N., 1989. Earthquakes associated with diffuse zones of deformation in the oceanic lithosphere: some examples, *Tectonophysics,* **166,** 133–150.

Chu, D. & Gordon, R.G., 1998. Current plate motions across the Red Sea, *Geophys. J. Int.,* **135,** 313–328.

Chu, D. & Gordon, R.G., 1999. Evidence for motion between Nubia and Somalia along the Southwest Indian ridge, *Nature,* **398,** 64–67.

Davies, R., England, P., Parsons, B., Billiris, H., Paradissis, D. & Veis, G., 1997. Geodetic strain in Greece in the interval 1892–1992, *J. geophys. Res.,* **102,** 24 571–24 588.

DeMets, C., Gordon, R., Argus, D.F. & Stein, S., 1990. Current plate motions, *Geophys. J. Int.,* **101,** 425–478.

DeMets, C., Gordon, R., Argus, D.F. & Stein, S., 1994. Effects of recent revisions to the geomagnetic time scale on estimates of current plate motion, *Geophys. Res. Lett.,* **21,** 2191–2194.

Dercourt, J. *et al.*, 1986. Geological evolution of the Tethys belt from the Atlantic to the Pamirs since the Lias, *Tectonophysics,* **123,** 241–315.

Dewey, J.F., Hempton, M.R., Kidd, W.S.F., Saroglu, F. & Sengor, A.M.C., 1986. Shortening of continental lithosphere: the neotectonics of eastern Anatolia—a young continental collision zone, in *Collision Tectonics,* Vol. 19, pp. 3–36, eds Coward, M.P. & Ries, A.C., Geol. Soc. Spec. Publ.

Dewey, J.F., Helman, M.L., Turco, E., Hutton, D.H.W. & Knott, S.D., 1989. in *Alpine Tectonics,* Vol. 45, pp. 265–283, eds Coward, M.P., Dietrich, D. & Park, R.G., Geological Society London, Special Publication.

Dong, D., Herring, T.A. & King, R.W., 1998. Estimating regional deformation from a combination of space and terrestrial geodetic data, *J. Geod.,* **72,** 200–211.

Goldsworthy, M., Jackson, J. & Haines, J., 2002. Continuity of active fault systems in Greece, *Geophys. J. Int.,* **148,** 596–618.

Gomez, F., Beauchamp, W. & Barazangi, M., 2000. Role of the Atlas Mountains (northwest Africa) within the Africa–Eurasia plate-boundary zone, *Geology,* **28,** 775–778.

Gomez, F. *et al.,* 2001. Coseismic displacements along the Serghaya fault: an active branch of the Dead Sea fault system in Syria and Lebanon, *J. geol. Soc. Lond.,* **158,** 405–408.

Gutscher, M.-A., Malod, J., Rehault, J.-P., Contrucci, I., Klingelhoefer, F., Mendes-Victor, L. & Spakman, W., 2002. Evidence for active subduction beneath Gibraltar, *Geology,* **30,** 1071–1074.

Hempton, M.R., 1987. Constraints on Arabia Plate motion and extensional history of the Red Sea, *Tectonics,* **6,** 687–705.

Herring, T.A., 1999. GLOBK: global Kalman filter VLBI and GPS analysis program version 4.1, Mass. Inst. of Technol., Cambridge.

Jackson, J. & McKenzie, D., 1984. Active tectonics of the Alpine–Himalayan Belt between western Turkey and Pakistan, *Geophys. J. R. astr. Soc.,* **77,** 185–246.

Jackson, J. & McKenzie, D., 1988. The relationship between plate motions and seismic moment tensors, and the rates of active deformation in the Mediterranean and Middle East, *Geophys. J. R. astr. Soc.,* **93,** 45–73.

Jackson, J., Haines, J. & Holt, W., 1995. The accommodation of Arabia–Eurasia plate convergence in Iran, *J. geophys. Res.,* **100,** 15 205–15 219.

Jestin, F., Huchon, P. & Gaulier, J.M., 1994. The Somalia Plate and the East Africa rift system: present-day kinematics, *Geophys. J. Int.,* **116,** 637–654.

Joffe, S. & Garfunkel, Z., 1987. Plate kinematics of the circum Red Sea—a re-evaluation, *Tectonophysics,* **141,** 5–22.

Jolivet, L. & Faccenna, C., 2000. Mediterranean extension and the Africa–Eurasia collision, *Tectonics,* **19,** 1095–1106.

Kahle, H.-G., Concord, M., Peter, Y., Geiger, A., Reilinger, R., Barka, A. & Veis, G., 2000. GPS derived strain rate field within the boundary zones of the Eurasian, African, and Arabian plates, *J. geophys. Res.,* **105,** 23 353–23 370.

King, R.W. & Bock, Y., 1999. Documentation for GAMIT analysis software, release 9.7, Mass. Inst. of Technol., Cambridge.

Klemper, D. & Ben-Avraham, Z., 1987. The tectonic evolution of the Cyprean arc, *Anneles Tectonica,* **1,** 58–71.

Klinger, Y., Avouac, J.P., Abou Karaki, N., Dorbath, L., Bourles, D. & Reyss, J.L., 2000. Slip rate on the Dead Sea transform fault in northern Araba valley (Jordan), *Geophys. J. Int.,* **142,** 755–768.

Larson, K.M., Freymueller, J.T. & Philipsen, S., 1997. Global plate velocities from the Global Positioning System, *J. geophys. Res.,* **102,** 9961–9981.

Le Pichon, X. & Angelier, J., 1979. The Hellenic arc and trench system: a key to the neotectonic evolution of the eastern Mediterranean area, *Tectonophysics,* **60,** 1–42.

Le Pichon, X., Chamot-Rooke, N., Lallemant, S., Noomen, R. & Veis, G., 1995. Geodetic determination of the kinematics of central Greece with respect to Europe: implications for eastern Mediterranean tectonics, *J. geophys. Res.,* **100,** 12 675–12 690.

Lyberis, N., 1988. Tectonic evolution of the Gulf of Suez and the Gulf of Aqaba, *Tectonophysics,* **153,** 209–220.

McClusky, S. *et al.,* 2000. GPS constraints on plate kinematics and dynamics in the eastern Mediterranean and Caucasus, *J. geophys. Res.,* **105,** 5695–5719.

McKenzie, D.P., 1972. Active tectonics of the Mediterranean region, *Geophys. J. R. astr. Soc.,* **30,** 109–185.

Malverno, A. & Ryan, W.B.F., 1986. Extension in the Tyrranean Sea and shortening in the Apennines as a result of arc migration driven by sinking of the lithosphere, *Tectonics,* **5,** 227–245.

Meade, B.J., Hager, B.H., McClusky, S., Reilinger, R.E., Ergintav, S., Lenk, O., Barka, A. & Ozener, H., 2002. Estimates of seismic potential in the Marmara region from block models of secular deformation constrained by Global Positioning System measurements, *Bull. seism. Soc. Am.,* **92,** 208–215.

Nocquet, J.-M., Calais, E., Altamimi, Z., Sillard, P. & Boucher, C., 2001. Intraplate deformation in western Europe deduced from an analysis of the International Terrestrial Reference Frame 1997 (ITRF97) velocity field, *J. geophys. Res.,* **106,** 11 239–11 257.

Papazachos, B.C. & Papaioannou, Ch.A., 1999. Lithospheric boundaries and plate motions in the Cyprus area, *Tectonophysics,* **308,** 193–204.

Pe'eri, S., Wdowinski, S., Shtibelman, A., Bechor, N., Bock, Y., Nikolaidis, R. & van Domselaar, M., 2002. Current plate motion across the Dead Sea

fault from three years of continuous GPS monitoring, *Geophys. Res. Lett.,* **29,** DOI10.1029/2001 GL013 879.

Philip, H., Cisternas, A., Gvishiani, A. & Gorshkov, A., 1989. The Caucasus: an actual example of the initial stages of continental collision, *Tectonophysics,* **161,** 1–21.

Quennell, A.M., 1984. The western Arabia rift system, in *The Geological Evolution of the Eastern Mediterranean,* Vol. 17, pp. 775–788, eds Dixon, J.E. & Robertson, A.H.F., Geological Society London, Special Publication.

Reilinger, R.E., McClusky, S.C., Souter, B.J., Hamburger, M.W., Prilepin, M.T., Mishin, A., Guseva, T. & Balassanian, S., 1997. Preliminary estimates of plate convergence in the Caucasus collision zone from global positioning system measurements, *Geophys. Res. Lett.,* **24,** 1815–1818.

Robins, J.W., Dunn, P.J., Torrence, M.H. & Smith, D.E., 1995. Deformation in the eastern Mediterranean, in *Proc. 1st Turkish Int. Symp. on Deformations,* Vol. 2, pp. 738–745, Chamber of Surv. Eng., Ankara, Turkey.

Royden, L., 1993. The tectonic expression of slab pull at continental convergent boundaries, *Tectonics,* **12,** 303–325.

Savelli, C., 2002. Time-space distribution of magmatic activity in the western Mediterranean and peripheral orogens during the past 30 Ma (a stimulus to geodynamic considerations), *J. Geodyn.,* **34,** 99–126.

Seber, D., Barazangi, M., Ibenbrahim, A. & Demnati, A., 1996. Geophysical evidence for lithospheric delamination beneath the Alboran Sea and Rif-Betic mountains, *Nature,* **379,** 785–790.

Sella, G.F., Dixon, T.H. & Mao, A., 2002. REVEL: a model for recent plate velocities from space geodesy, *J. geophys. Res.,* **107,** B4, 10.1029/2000 JB000 033.

Sengor, A.M.C., 1979. The North Anatolian transform fault: its age, offset, and tectonic significance, *J. geol. Soc. Lond.,* **136,** 269–282.

Sengor, A.M.C., Gurur, N. & Saroglu, F., 1985. Strike slip faulting and related basin formation in zones of tectonic escape: Turkey as a case study, in *Strike Slip Faulting and Basin Formation,* Vol. 37, pp. 227–264, eds Biddle, K.T. & Christie-Blick, N., Spec. Publ. Econ. Paleontol. Mineral.

Steckler, M.S., Berthelot, F., Lyberis, N. & Le Pichon, X., 1988. Subsidence in the Gulf of Suez: implications for rifting and plate kinematics, *Tectonophysics,* **153,** 249–270.

Steckler, M.S., Feinstein, S., Kohn, B.P., Lavier, L.L. & Eyal, M., 1998. Pattern of mantle thinning from subsidence and heat flow measurements in the Gulf of Suez: evidence for the rotation of the Sinai and along-strike flow from the Red Sea, *Tectonics,* **17,** 903–920.

Tatar, M., Hatzfeld, D., Martinod, J., Walpersdorf, A., Ghafori-Ashtiany, M. & Chery, J., 2002. The present-day deformation of the central Zagros from GPS measurements, *Geophys. Res. Lett.,* **29,** 10.1029/2002 GL015 427.

Taymaz, T., Eyidogan, H. & Jackson, J., 1991. Source parameters of large earthquakes in the East Anatolian fault zone (Turkey), *Geophys. J. Int.,* **106,** 537–550.

Thatcher, W., 1995. Microplate versus continuum descriptions of active tectonic deformation, *J. geophys. Res.,* **100,** 3885–3894.

Udias, A., Lopez Arroyo, A. & Mezcua, J., 1976. Seismotectonics of the Azores–Alboran region, *Tectonophysics,* **31,** 259–289.

Wessel, P. & Smith, W.H.F., 1995. New version of the generic mapping tools released, *EOS, Trans. Am. geophys. Un.,* **76,** 329.

Westaway, R., 1994. Present-day kinematics of the Middle East and eastern Mediterranean, *J. geophys. Res.,* **99,** 12 071–12 090.

Wortel, M.J.R. & Spakman, W., 2000. Subduction and slab detachment in the Mediterranean–Carpathian region, *Science,* **290,** 1910–1917.